Int J Thermophys (2016) 37:60
DOI 10.1007/s10765-016-2065-x

ICPPP 18

Trap State Effects in PbS Colloidal Quantum Dot Exciton Kinetics Using Photocarrier Radiometry Intensity and Temperature Measurements

Jing Wang[1] · **Andreas Mandelis**[1,2] · **Alexander Melnikov**[2] · **Qiming Sun**[1]

Received: 11 October 2015 / Accepted: 15 April 2016 / Published online: 28 April 2016

Abstract Colloidal quantum dots (CQDs) have attracted significant interest for applications in electronic and optoelectronic devices such as photodetectors, light-emitting diodes, and solar cells. However, a poor understanding of charge transport in these nanocrystalline films hinders their practical applications. The photocarrier radiometry (PCR) technique, a frequency-domain photoluminescence method spectrally gated for monitoring radiative recombination photon emissions while excluding thermal infrared photons due to non-radiative recombination, has been applied to PbS CQD thin films for the analysis of charge transport properties. Linear excitation intensity responses of PCR signals were found in the reported experimental conditions. The type and influence of trap states in the coupled PbS CQD thin film were analyzed with PCR temperature- and time-dependent results.

Keywords Charge transport · PbS colloidal quantum dots · Photocarrier radiometry · Temperature response · Trap states

ICPPP 18 Topical Collection.

✉ Jing Wang
s.j19851230@163.com

[1] School of Optoelectronic Information, University of Electronic Science and Technology of China, Chengdu, Sichuan 610054, China

[2] Center for Advanced Diffusion-Wave Technologies (CADIFT), Department of Mechanical and Industrial Engineering, University of Toronto, Toronto M5S 3G8, Canada

1 Introduction

Lead-salt colloidal quantum dots (CQDs) have been successfully employed as active components in electronic and optoelectronic devices such as photodetectors [1,2], light-emitting diodes [3,4] and solar cells [5,6]. Studies of lead-salt CQDs have received great attention during the past 20 years and still attract a growing number of investigations from both fundamental and applied points of view. From the fundamental point of view, such materials are great candidates to probe the strong quantum confinement effects, due to the large exciton Bohr radius (17.4 nm) [7], narrow band gap [8], and nearly equivalent electron and hole effective masses [8]. From the technology aspect, this type of CQDs provides tunable electronic transitions in the spectral range from near infrared to visible, and shows multiple exciton generation effects [9,10], a mechanism that could potentially lead to improved solar conversion efficiencies. However, a poor understanding of charge transport in these nanocrystalline films hinders their practical applications. Carrier dynamics involving trap states in CQDs have been studied with temperature-dependent photoluminescence properties. Gaponenko et al. reported the lowest exciton state splitting and carrier trapping in PbS QDs in a glass matrix by temperature-dependent photoluminescence measurements [11]. Andreakou et al. proposed a three-level system composed of bright, dark, and surface states, which describes the observed temperature-dependent photoluminescence dynamics of oleic acid-capped PbS QDs [12]. In the report by Pendyala et al., the nature of surface states was revealed also by temperature-dependent photoluminescence studies [13]. Bakulin et al. applied pump-push photocurrent spectroscopy to elucidate the charge trapping dynamics in PbS CQD solar cells at working conditions. Using IR photoinduced absorption as a probe, they observed that the early trapping dynamics strongly depend on the nature of the ligands used for QD passivation [14]. Unlike ultrafast pump-push photocurrent spectroscopy which targets very early trapping dynamics, photocarrier radiometry (PCR), as a dynamic spectrally integrated frequency-domain PL modality, has been applied to test radiative and non-radiative relaxation lifetime distributions in PbS CQDs on relatively long time scales ($\sim\mu$s) commensurate with effective dielectric screening. Superior frequency-domain PCR accuracy and precision to time-resolved PL is due to its intrinsically high signal-to-noise ratio (SNR) based on narrowband lock-in demodulation [15,16]. Studies demonstrated that PCR is a powerful tool for analysis of exciton transport and relaxation properties in QDs. In this work, PCR laser intensity-, temperature- and time-dependent measurements were carried out in order to offer insight into the energy level of surface trap states caused by different passivation methods applied to the PbS CQDs.

2 Materials, Instrumentation, and Experimental Results

Two PbS CQD samples were studied for the purpose of probing excitonic carrier transport properties in QDs. Both thin-film samples contained PbS colloidal quantum dots with a mean diameter of 4.2 nm. The first (“uncoupled”) sample was fabricated through drop casting of oleic acid-capped PbS QDs. The large inter-particle spacing of 4.2 nm

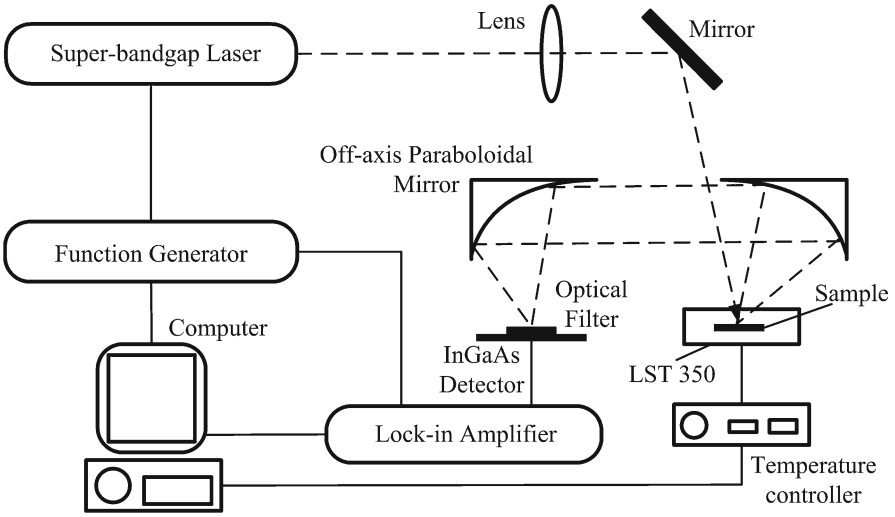

Fig. 1 Schematic diagram of the photocarrier radiometry (PCR) set-up for CQD temperature and time scans

does not allow strong interactions between dots and hence the QDs were uncoupled. The second ("coupled") sample was fabricated through a layer-by-layer process in which the long oleic acid ligands were displaced by shorter 3-mercaptopropionic acid ligands, resulting in an inter-particle spacing of about 0.5–1 nm. Such spacing allows for strong interactions between dots resulting in a coupled QD system. Halide anions were used to bind hard-to-access sites. As reported by Sargent's group, in such kinds of coupled samples the midgap trap state density is at least five times lower than in uncoupled samples [17].

The schematic diagram of the PCR experimental set-up was similar to our previous publications [15,16] and is shown in Fig. 1. A 100 mW diode laser with a wavelength of 830 nm and a beam diameter of *ca.* 0.1 mm was square-wave modulated with a function generator. A 1 μm long-pass filter was placed in front of the InGaAs photodetector to block the excitation beam. No short-pass filter was necessary as thermal infrared contributions to the signal were found to be negligible. The sample was placed on a Linkam LTS350 cryogenic stage, which allows maintaining constant temperature in the 77–520 K range. Since high temperatures may dramatically and irreversibly change the properties of the PbS CQDs, the highest temperature for frequency and temperature scans was set to 300 K.

Laser intensity responses of PCR signals were carried out for three different temperatures (300 K, 200 K, and 100 K) at fixed laser modulation frequency (1 kHz). A variable neutral density filter was set on the path of the output laser beam to gradually adjust the illumination intensity on the samples. Temperature scans of PCR signals were performed using a cooling rate of 10°C/min for three different laser modulation frequencies (1 kHz, 10 kHz, and 100 kHz) with fixed laser power (30 mW). The temperature scan range was from 300 K to 100 K. PCR time response measurements were

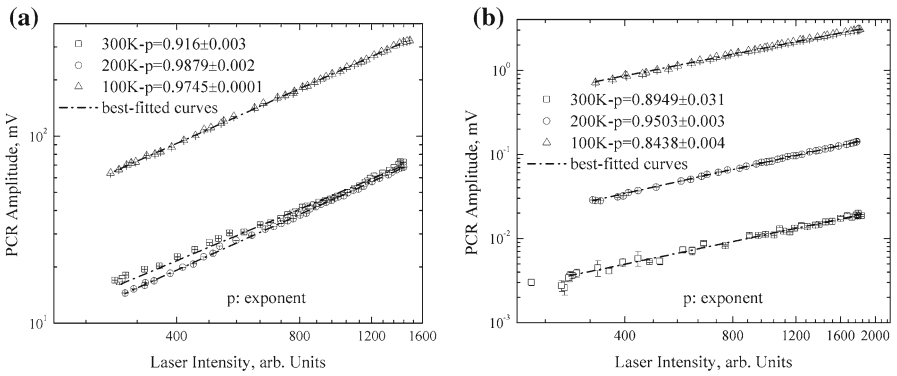

Fig. 2 PCR laser intensity scan curves for both PbS CQD samples at various temperatures. Best fitted curves were calculated from Eq. 1. (a) Uncoupled sample and (b) coupled sample. p is the exponent in Eq. 1

also carried out at five different temperatures (300 K, 250 K, 200 K, 150 K, and 100 K) with fixed laser power (30 mW) and modulation frequency (1 kHz).

3 Results and Discussion

3.1 PCR Excitation Intensity Response

Figure 2 shows the excitation intensity response of the PCR amplitude of both PbS CQD samples at various temperatures. The experimental responses were fitted with Eq. 1. The exponents were found to be close to 1, indicating that the PCR signals are approximately linear in pump laser intensity. This is the basis of validation of other linear PCR theories in QD studies [18].

$$y = ax^p + c \tag{1}$$

3.2 PCR Temperature Response

Figure 3 shows the PCR temperature response of the two samples in Arrhenius plots. For both samples, decreasing temperature leads to pronounced growth of the PCR amplitude because of decreased non-radiative recombination probability at lower temperatures, which scales with phonon population. Similar trends in transient PL intensity emitted by PbS QDs and Si QDs were observed by P. Andreakou et al. [12] and Wen et al. [19]. The larger low-temperature PCR phase lag with increasing frequency is consistent with increased excitonic de-excitation lifetimes.

Invoking the photo-thermal rate-window concept [20,21], the PL efficiency can by approximated by

$$I(T) / I_0 = \frac{P_R}{P_R + P_{NR}}, \tag{2}$$

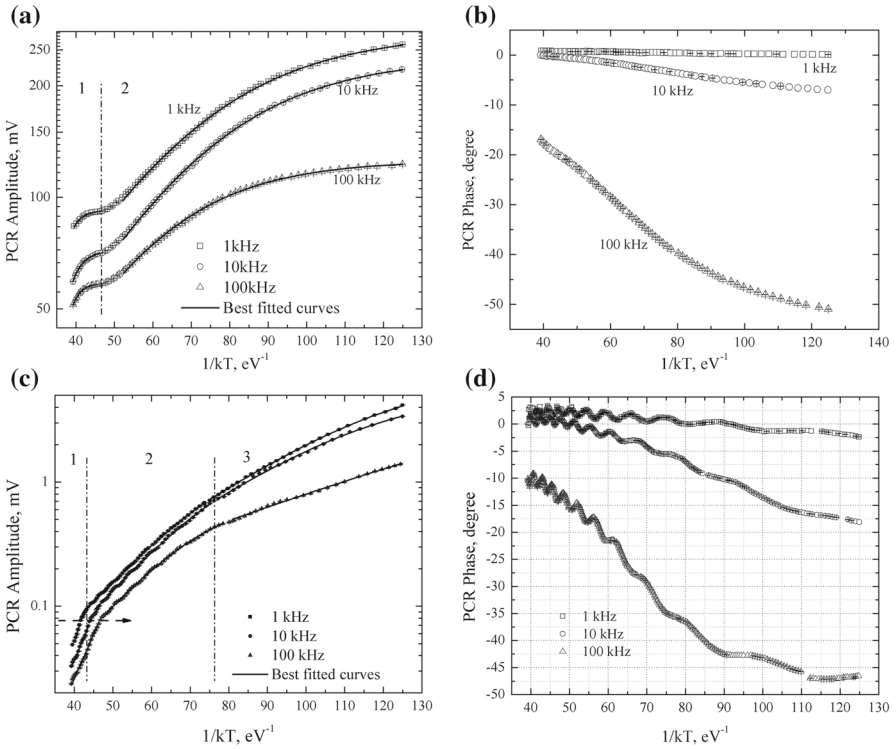

Fig. 3 PCR photo-thermal spectra (temperature scan curves) for both PbS CQD samples at various frequencies. Best fitted curves were calculated from Eq. 4. (a) Amplitude of uncoupled sample, (b) phase of uncoupled sample, (c) amplitude of coupled sample, and (d) phase of coupled sample. Dash dot lines are there to guide the eye between thermal activation regions

where P_R and P_{NR} are the radiative and non-radiative recombination probabilities, respectively. I(T) is the luminescence intensity and I_0 is the normalizing factor. It is normally assumed (but is not always true) that P_R is a constant and P_{NR} can be thermally activated:

$$P_{NR}(T) = P_{NR0} \exp\left(-E_a / k_B T\right). \tag{3}$$

Here E_a is the activation energy for non-radiative recombination which can be greatly affected by the existence of defect states. T is the absolute temperature and k_B is the Boltzmann constant. Substituting Eqs. 3 into 2 yields

$$I = I_0/(1 + A \exp\left(-E_a / k_B T\right)), \tag{4}$$

where $A \equiv P_{NR0} / P_R$ is a constant. Using Eq. 4 to fit the PCR amplitude signals in Fig. 3a, covering the entire temperature scan range is not appropriate as multiple trends are obvious in each curve. The signals from the uncoupled sample (Fig. 3a) were divided by an auxiliary line (dash dot line) into two sections, while the signals of the coupled sample (Fig. 3c) were divided into three sections. Among various possibilities of multiple thermally activated processes, these temperature range selections were

Table 1 Summary of best fitted values of non-radiative recombination activation energies in both samples

Frequency (kHz)	Uncoupled sample		Coupled sample		
	E_{a1} (meV)	E_{a2} (meV)	E_{a1} (meV)	E_{a2} (meV)	E_{a3} (meV)
1	443.2	43.4	238.8	77.6	48.6
10	387.1	45.4	172.9	78.7	48.9
100	503.6	51.8	162.5	82.4	26.9

based on a hypothesis of trap state contributions to the kinetics of excitons and criteria of good fitting to the data, and the fitting results for the activation energies were consistent with reported literature values.

By fitting the experimental data in each section with Eq. 4, the activation energies of non-radiative recombinations over the corresponding temperature ranges were obtained at each frequency as shown in Table. 1, where traps of different activation energies E_{ai} were assumed. It was found that E_{a1} is much higher than E_{a2} at every frequency for the uncoupled sample, thus indicating that deep-level trap states dominate non-radiative recombination at higher temperatures since excitons in shallow trap states can easily return to free exciton states through thermal emission. When temperature decreases, shallow trap states affect non-radiative recombination more strongly due to the smaller amounts of energy available for thermal emissions from the traps. E_{a1} of the uncoupled sample is much higher than that of the coupled sample, which indicates that for the uncoupled sample excitons occupy deeper states than in the coupled sample at the same temperature. This is consistent with the relative surface trapping properties [17] of these two PbS thin films with the midgap trap density in the coupled sample being five times lower than that in the uncoupled sample.

Knee points on the amplitude curves of the coupled sample shift to lower temperatures when laser modulation frequency increases, as shown with the arrow in Fig. 3c. The temperature scan at fixed modulation frequencies is a form of a rate-window photo-thermal spectrum [20]. Physically, this is a thermal spectroscopy resonance phenomenon marked by a PCR signal extremum or change in the Arrhenius plot slope at temperatures where the carrier emission rate from a trap matches the frequency of observation as set in the lock-in amplifier. Equation 3 shows that higher thermal emission rates occur at higher temperatures and/or from traps with lower activation energies. In this rate-window picture, the shift of the change in the amplitude slope to a different temperature indicates the domination of a different emission process in the new temperature range. Figure 3a, c shows that there may be two or more trap states active with contributions to the non-radiative relaxation which decreases the (radiatively recombining) photocarriers with increasing temperature. The best fitted amplitude results are shown in Table 1. The PCR phases, Fig. 3b, d, corroborate the amplitude behavior by exhibiting larger lags at lower temperatures at fixed modulation frequency (characteristic of increased lifetimes as expected [16]), and more pronounced changes in slope at higher frequencies as the energetic location of the recombining carrier source shifts across different trap states. Unfortunately, unlike the case with semi-insulating GaAs [20,21], at this time we have no fully developed

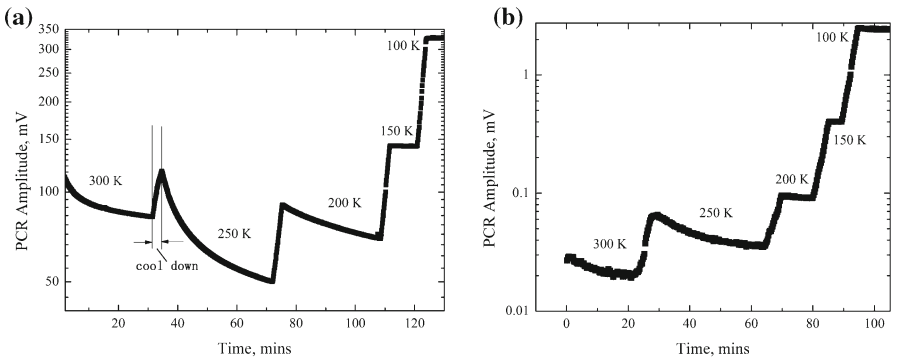

Fig. 4 PCR time scan amplitude signals for both PbS CQD samples at various temperatures. (a) Uncoupled sample and (b) coupled sample

model of the effects of thermal emissions from traps in CQDs to perform quantitative fits to the phase spectra of Fig. 3b, d.

Another noteworthy phenomenon of the temperature response in the coupled sample is the oscillating behavior superposed on the phase curves at all frequencies (Fig. 3d). The amplitude curves (Fig. 3c) also show some degree of oscillation, but this is not as evident as in the phase curves. The origin of the oscillations remains unknown and is subject to further investigations which will take into account the electrical behavior of solar cell devices fabricated from coupled colloidal quantum nanolayers.

3.3 Time-Dependent PCR Responses

In the course of the foregoing experiments, it was observed that PCR signals change with time with no change in any of the experimental conditions. Time responses of PbS CQDs at five different temperatures were monitored, and the samples required different amounts of time at different temperatures in the cryostat for the PCR amplitude to stabilize. The temperature and intensity scans (Figs. 2, 3) were carried out after laser exposure of the samples for at least 1 hour. As a result, the PCR experiments were performed in a relatively steady state, because transient PCR signal changes did not affect the fast temperature-dependent responses. Following signal stabilization (or nearly so), the temperature was changed at different cooling rates; for instance, a 15 K/min cooling rate was used from 300 K to 250 K. The results are shown in Fig. 4. Both samples exhibit obvious transients, decreasing with time at high temperatures ($T \geq 200\,K$) for approx. 20 min, and become time independent at lower temperatures. This is consistent with the presence of non-radiative trap states which capture excitons, resulting in PL quenching. Such states (especially shallow traps) are most likely empty (unoccupied) at high temperatures owing to thermal emission. In this picture, the transients observed at high temperatures are functions of a combination of kinetics involving emission and capture rates [21]. The long time constant of the transient indicates that the exciton capture and emission processes into and from traps are slow (rate limiting) compared to exciton generation and recombination. The PCR

signals increase as temperature decreases due to the decrease of non-radiative recombination probability as shown in Eq. 3. At the same time, the thermal emission and capture processes become less efficient and radiative recombinations dominate exciton kinetics. The result is the considerable decrease in the PCR amplitude transient time constant which ultimately becomes infinitesimal within the observation period at temperatures below 200 K. Comparing Fig. 4a, b, it was found that the transient time constants of the PCR amplitudes at high temperatures in the uncoupled sample were longer than those in the coupled sample. This is consistent with the deeper trap states (higher activation energies) identified for this sample (Table 1), into and out of which exciton capture and thermal emission rates are significantly lower than those in the coupled sample. This is also consistent with the presence of deep surface excitonic trap states generated by capping with oleic acid by a surface passivation method [17].

4 Conclusions

The temperature and time dependences of PCR measurements with uncoupled and coupled PbS colloidal quantum dot nanolayers were studied. Trap energetics and thermal emission activation energies were calculated using the photo-thermal rate-window concept. In a simple non-radiative recombination model, much larger exciton trap thermal activation energies than coupled CQDs were found for the uncoupled PbS CQDs which are capped with oleic acid, thereby creating deeper surface trap states. Photo-thermal emission spectra and kinetic transients were studied using the PCR signal amplitude. The spectra were found to be consistent with a physical picture of significant recombination lifetime effects of thermal (non-radiative) trapping and emission at temperatures equal to, or higher than, 200 K for both types of samples, but the effects were more pronounced in the case of the uncoupled sample due to the higher trapping/detrapping activation energies involved. The effects were negligible at lower temperatures for both samples, in agreement with prior PCR studies of PbS CQDs [16].

Acknowledgments A. Mandelis is grateful to the Natural Sciences and Engineering Research Council (NSERC) for a Discovery grant, to the Canada Foundation for Innovation (CFI) for equipment grants, to the Canada Research Chairs Program, to the Ontario Ministry for Research and Innovation (MRI) for the Inaugural Premier's Discovery Award in Science and Technology (2007), and to the Chinese Recruitment Program of Global Experts (Thousand Talents). J. Wang is grateful to the National Natural Science Foundation of China (Grant No. 61379013). Sjoerd Hoogland and Edward H. Sargent are acknowledged for CQD sample contributions.

References

1. J.P. Clifford, G. Konstantatos, K.W. Johnston, S. Hoogland, L. Levina, E.H. Sargent, Nat. Nanotechnol. **4**, 40 (2009)
2. G. Konstantatos, I. Howard, A. Fischer, S. Hoogland, J.P. Clifford, E. Klem, L. Levina, E.H. Sargent, Nature **442**, 180 (2006)
3. S. Coe, W.K. Woo, M. Bawendi, V. Bulovic, Nature **420**, 800 (2002)
4. A.H. Mueller, M.A. Petruska, M. Achermann, D.J. Werder, E.A. Akhadov, D.D. Koleske, M.A. Hoffbauer, V.I. Klimov, Nano Lett. **5**, 1039 (2005)

5. K.W. Johnston, A.G. Pattantyus-Abraham, J.P. Clifford, S.H. Myrskog, D.D. MacNeil, L. Levina, E.H. Sargent, Appl. Phys. Lett. **92**, 151115 (2008)
6. S.A. McDonald, G. Konstantatos, S. Zhang, P.W. Cyr, E.J.D. Klem, L. Levina, E.H. Sargent, Nat. Mater. **4**, 138 (2005)
7. J.E. Murphy, M.C. Beard, A.G. Norman, SPh Ahrenkiel, J.C. Johnson, P. Yu, O.I. Mii, R.J. Ellingson, A.J. Nozik, J. Am. Chem. Soc. **128**, 3241 (2006)
8. O. Madelung, *Semiconductors: Data Handbook*, 3rd edn. (Springer, Berlin, 2004)
9. R.J. Ellingson, M.C. Beard, J.C. Johnson, P. Yu, O.I. Micic, A.J. Nozik, A. Shabaev, A.L. Efros, Nano Lett. **5**, 865 (2005)
10. D.J. Farrell, Y. Takeda, K. Nishikawa, T. Nagashima, T. Motohiro, N.J. Ekins-Daukes, Appl. Phys. Lett. **99**, 111102 (2011)
11. M.S. Gaponenko, A.A. Lutich, N.A. Tolstik, A.A. Onushchenko, A.M. Malyarevich, E.P. Petrov, K.V. Yumashev, Phys. Rev. B **82**, 125320 (2010)
12. P. Andreakou, M. Brossard, C.Y. Li, M. Bernechea, G. Konstantatos, P.G. Lagoudakis, J. Phys. Chem. C **117**, 1887 (2013)
13. N.B. Pendyala, K.S.R.K. Rao, J. Lumin. **128**, 1826 (2008)
14. A.A. Bakulin, S. Neutzner, H.J. Bakker, L. Ottaviani, D. Barakel, Z. Chen, ACS Nano. **7**(10), 8771 (2013)
15. J. Wang, A. Mandelis, J. Phys. Chem. C **118**, 19484 (2014)
16. J. Wang, A. Mandelis, A. Melnikov, S. Hoogland, E.H. Sargent, J. Phys. Chem. C **117**, 23333 (2013)
17. A.H. Ip, S.M. Thon, S. Hoogland, O. Voznyy, D. Zhitomirsky, R. Debnath, l Levina, Nat. Nanotechnol. **7**, 577 (2012)
18. Q. Sun, A. Melnikov, A. Mandelis, in *Proceedings of the 40 th IEEE Photovoltaic Specialists Conference*, pp. 1860–1865 (2014). doi:10.1109/PVSC.2014.6925287
19. X. Wen, L.V. Dao, P. Hannaford, J. Phys. D **40**, 3573 (2007)
20. J. Xia, A. Mandelis, Appl. Phys. Lett. **96**, 262112 (1–3) (2010)
21. J. Xia, A. Mandelis, Appl. Phys. Lett. **90**, 062119 (1–3) (2007)